Emission from an active photonic crystal

I. El-Kady, W. W. Chow, and J. G. Fleming
Sandia National Laboratories, P.O. Box 5800, Albuquerque, New Mexico 87185-0601, USA
(Received 19 September 2005; published 22 November 2005)

We investigated theoretically the emission from an active photonic crystal. Redistribution of photon density of states by a photonic lattice was found to greatly influence the thermal emission spectrum, resulting in substantial deviation from the Planck distribution. The calculation predicts that the photonic lattice intensity may exceed that of a blackbody source within certain spectral regions. However, the excess emission may be lost in practice because of nonradiative losses and photonic lattice inhomogeneities.

DOI: 10.1103/PhysRevB.72.195110 PACS number(s): 42.70.Qs, 42.55.Tv, 44.40.+a, 78.67.Hc

I. INTRODUCTION

In the presence of a photonic crystal host, a multitude of novel optical phenomena arise because of two main features of a photonic lattice band structure: suppression of photon density of states along certain crystallographic directions and propagation of selected Bloch-modes as mandated by translational symmetry. Examples of novel phenomena include, inhibition of spontaneous emission,[1,2] reduced group velocity,[3] exceedingly high cavity-Q factors,[4] low threshold lasing,[5] and modified emission characteristics.[6,7] This paper focuses on the last phenomenon, where it was shown that a dielectric photonic crystal can funnel thermal radiation into narrow radiation bands.[7] While there are theoretical and experimental results indicating exceedingly high intensities at the photonic lattice band edge, the question of whether these intensities exceed those of a blackbody at the same temperature and wavelength is unresolved.[6,8,9] An answer is important for scientific understanding and engineering development of a new generation of optical sources and detectors whose properties may go beyond the standard quantum limits. A problem with arriving at an answer experimentally is the difficulty in ensuring that the comparison is made under the same conditions.

The aim of this study is to address the question of thermal radiation from photonic lattices theoretically. Our approach begins with a first-principles calculation of the photonic lattice band structure. The results are used in a model of an active photonic crystal consisting of an inhomogeneously broadened ensemble of two-level systems interacting with a quantized multimode radiation field, whose modal properties are determined by the photonic lattice band structure.[10] The composite system is excited by an external pump and allowed to equilibrate with a thermal bath via collisions.

Section II describes the theoretical model, where approximations are made to facilitate the comparison of photonic crystal and blackbody emissions. Results are presented in Sec. III for the limiting cases determined by experimental conditions. To evaluate the model, we show that it retrieves Planck's blackbody distribution in the absence of a photonic crystal, and that the emission peak wavelengths and relative intensities are consistent with experimental values obtained for a lattice subjected to similar conditions.

II. THEORY

In formulating the problem, we label each two-level system with n, so that $|a_n\rangle$ and $|b_n\rangle$ are the ground and excited states, respectively, that are separated by energy $\hbar\omega_n$. Correspondingly, each radiation field mode has energy $\hbar\Omega_k$, and is described by creation and annihilation operators $a_k^\dagger$ and a_k, respectively. The relation between Ω_k and k depends on the photonic lattice structure. The Hamiltonian for the combined matter and radiation field system is[10,11]

$$H = \sum_n \hbar\omega_n |b_n\rangle\langle b_n| + \sum_k \hbar\Omega_k a_k^\dagger a_k - \sum_{k,n} g_k(|b_n\rangle\langle a_n| a_k + a_k^\dagger |a_n\rangle\langle b_n|), \quad (1)$$

where the dipole interaction is assumed, with

$$g_k = \mu\sqrt{\frac{\hbar\Omega_k}{\varepsilon_0 V}}, \quad (2)$$

μ is the dipole matrix element, ε_0 is the permittivity in vacuum, and V is the system volume. Introducing the operators for the microscopic polarization amplitude $\sigma_n^\dagger A_k \equiv |b_n\rangle\langle a_n| a_k \exp[-i(\omega_n - \Omega_k)t]$, the excited and ground state populations, $\sigma_{an} \equiv |a_n\rangle\langle a_n|$ and $\sigma_{bn} \equiv |b_n\rangle\langle b_n|$, respectively, and working in the Heisenberg picture, we derive

$$\frac{d\sigma_n^\dagger A_k}{dt} = \frac{i}{\hbar}\sum_{k'} g_{k'}(\sigma_{bn} A_k A_{k'}^\dagger - A_{k'}^\dagger A_k \sigma_{an}) e^{-i(\omega_n - \Omega_{k'})t}, \quad (3)$$

$$\frac{d\sigma_{an}}{dt} = \frac{i}{\hbar}\sum_k g_k(A_k^\dagger \sigma_n e^{-i(\omega_n - \Omega_{k'})t} - \sigma_n^\dagger A_k e^{i(\omega_n - \Omega_{k'})t}), \quad (4)$$

$$\frac{d\sigma_{bn}}{dt} = -\frac{i}{\hbar}\sum_k g_k(A_k^\dagger \sigma_n e^{-i(\omega_n - \Omega_{k'})t} - \sigma_n^\dagger A_k e^{i(\omega_n - \Omega_{k'})t}). \quad (5)$$

Additionally, the photon number operator obeys,

$$\frac{dA_k^\dagger A_k}{dt} = \frac{i}{\hbar}\sum_n g_k[A_k^\dagger \sigma_n e^{-i(\omega_n - \Omega_k)t} - \sigma_n^\dagger A_k e^{i(\omega_n - \Omega_k)t}]. \quad (6)$$

Assuming that the polarization dephasing rate γ is much faster than the time variations in the active medium and photon populations, one may adiabatically eliminate the polarization equation. Then, introducing the expectation values $n(\Omega, t) = \langle A_k^\dagger(t) A_k(t)\rangle$, $n_a(\omega_n, t) = \langle \sigma_{an}(t)\rangle$ and $n_b(\omega_n, t) = \langle \sigma_{bn}(t)\rangle$, we obtain the working equations for our analysis,

$$\frac{dn_a(\omega_n,t)}{dt} = \frac{2\pi}{\hbar^2}\rho(\omega_n)g(\omega_n)^2\{[n_b(\omega_n,t) - n_a(\omega_n,t)]n(\omega_n,t) + n_b(\omega_n)\} - \gamma_r[n_a(\omega_n,t) - f_a(\omega_n,t)] - \Lambda(\omega_n)n_a(\omega_n,t), \quad (7)$$

$$\frac{dn_b(\omega_n,t)}{dt} = -\frac{2\pi}{\hbar^2}\rho(\omega_n)g(\omega_n)^2\{[n_b(\omega_n,t) - n_a(\omega_n,t)]n(\omega_n,t) + n_b(\omega_n)\} - \gamma_r[n_b(\omega_n,t) - f_b(\omega_n,T)] + \Lambda(\omega_n)n_a(\omega_n,t), \quad (8)$$

$$\frac{dn(\Omega,t)}{dt} = \frac{2}{\hbar^2}g(\Omega)^2\sum_n \frac{\gamma}{(\omega_n-\Omega)^2+\gamma^2}\{[n_b(\omega_n,t) - n_a(\omega_n,t)]n(\Omega,t) + n_b(\omega_n,t)\} - \gamma_c n(\Omega,t), \quad (9)$$

where $\rho(\Omega)$ is the photonic-lattice density of states, which is assumed to be spherically symmetric. Additionally, the pump and decay contributions are included phenomenologically, where γ_c is the photon decay rate,

$$\Lambda(\omega_n) = \Lambda_0 \exp\left(-\frac{\hbar\omega_n}{k_B T_p}\right) \quad (10)$$

is the pump rate, and γ_r is the effective rate for the actual populations n_a and n_b to relax to the equilibrium distributions

$$f_a(\omega_n,T) = Z_o, \quad (11)$$

$$f_b(\omega_n,T) = Z_o \exp\left(\frac{-\hbar\omega_n}{k_B T}\right), \quad (12)$$

where Z_o is the thermodynamic partition function that is determined by the total number of two-level systems $N_o = \Sigma_n[f_a(\omega_n)+f_b(\omega_n)]$, T_p and T are the pump and reservoir temperatures. Solving Eqs. (7)–(9) gives the photon population inside the photonic lattice.

To relate to experiments, it is necessary to obtain the emission outside the photonic lattice. Theoretically, this is a nontrivial step because in our attempt to properly treat the active medium and its emission physics with a quantum theory, we relied on orthonormal optical modes for an infinite photonic lattice. This is very similar to a long-standing problem in laser theory.[12] There, one circumvents the issue by beginning with the Fox-Li modes for a Fabry-Perot cavity with perfectly reflecting mirrors, and then introducing a loss mechanism to represent the outcoupling.[13,14] Following this approach, we use the steady state solutions $n(\Omega,t) \rightarrow n(\Omega)$ in

$$u(\lambda) = \Gamma(\lambda)\frac{d\Omega}{d\lambda}\hbar\Omega_\rho(\Omega)n(\Omega) \quad (13)$$

to obtain the emission wavelength spectrum outside the photonic lattice enclosure, where

$$\Gamma(\lambda) = 1 - [R(\lambda) + A(\lambda)] \quad (14)$$

is the coupling factor describing the efficiency with which radiation inside the photonic crystal is coupled to the outside, $R(\lambda)$ is the reflectivity, $A(\lambda)$ is the absorption. The determination of $R(\lambda)$ and $A(\lambda)$ is described in the following section.

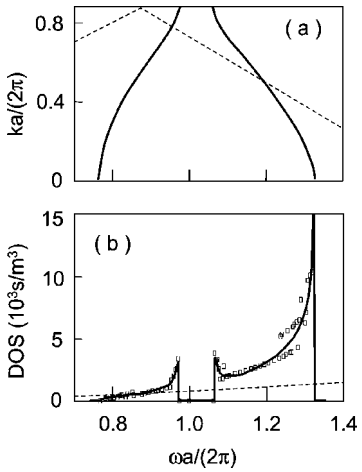

FIG. 1. (a) Calculated photonic-crystal (solid curve) and free-space (dashed curve) dispersions. (b) Densities of states computed from the photonic-crystal (dots) and free-space (dashed curves) dispersions in (a). The solid line is the least-squares fit to the dots.

III. RESULTS

In this study, we consider a tungsten Lincoln-log photonic crystal with 28.5% filling fraction and square cross-section rods. A coupled-wave method is used to compute the band structure, where the fields and dielectric functions are expanded in terms of plane waves. Maxwell's equations are cast in an eigen problem format in Fourier space and solved using a transfer matrix approach by treating each layer of the structure as an independent 2D Lamellar grating. Details of this method and its accuracy in describing our structure are discussed elsewhere.[15] The reflectivity $R(\lambda)$ and absorption $A(\lambda)$ are obtained by an independent frequency domain transfer matrix calculation performed on six layers of the photonic crystal structure.[16]

Figure 1(a) shows the photonic-lattice dispersion in the (001) crystallographic direction (solid curve). Clearly visible are the fundamental and first higher order gaps, as well as the significant flattening of the dispersion at the band edges due to anticrossing. The dots in Fig. 1(b) give the density of states (DOS) $\rho(\omega)$ computed from the dispersion, assuming spherical symmetry. Note the drastic increases in DOS as the photonic crystal dispersion flattens at the band edges. For comparison, Fig. 1 also shows the free-space dispersion and DOS (dashed curves).

Using the photonic-crystal DOS in Fig. 1(b), Eqs. (7)–(9) are solved numerically with a fourth-order Runge-Kutta finite difference method. Following previous comparisons of photonic crystal and blackbody emissions, we ensure that the steady-steady active-medium populations $n_a(\omega_n)$ and $n_b(\omega_n)$ are to a good approximation given by the equilibrium distributions $f_a(\omega_n,T)$ and $f_a(\omega_n,T)$ by performing the calculations for low excitation and rapid relaxation conditions, specifically, with $\gamma = 10^{14}$ s^{-1}, $\gamma_r = 10^{12}$ s^{-1}, and $\gamma_c = \Lambda_0 = 10^9$ s^{-1}. Furthermore, we choose $\mu = e \times 0.5$ nm, $V = 10^{-18}$ m^{-3}, $N_0 = 200$ and $T_p = T$. The steady-state solutions to Eqs. (7)–(9),

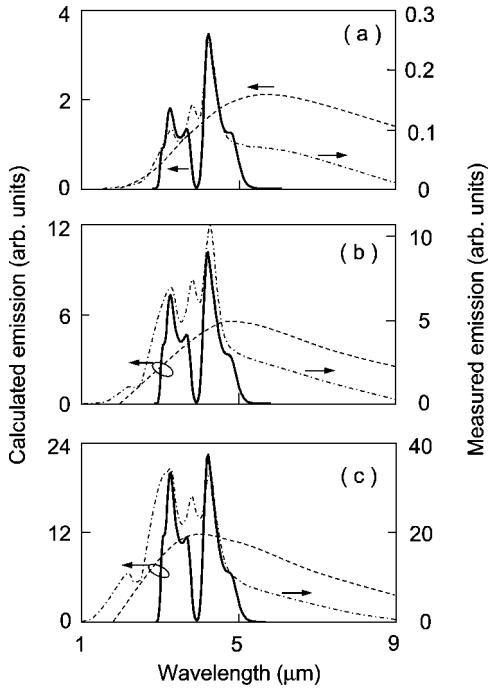

FIG. 2. Calculated blackbody (dashed curve) and lossless photonic-crystal (solid curve) emission spectra for $T=$(a) 500 K, (b) 600 K, and (c) 700 K. The dotted-dashed curves are the experimental spectra.

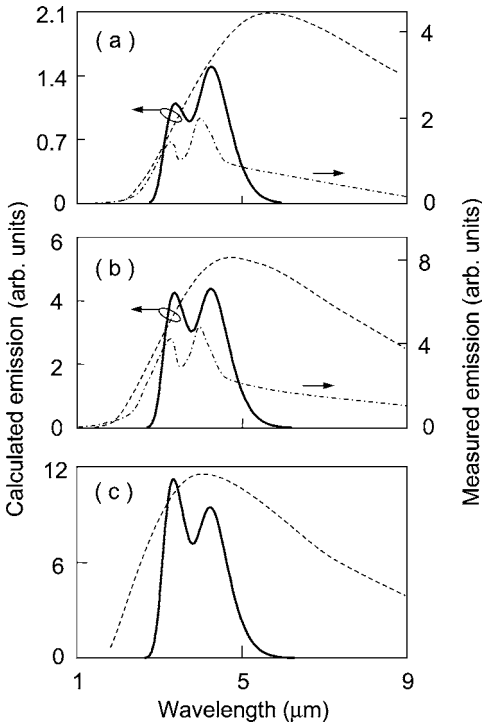

FIG. 3. Calculated blackbody (dashed curve) and lossy photonic-crystal (solid curve) emission spectra for $T=$(a) 500 K, (b) 600 K, and (c) 700 K. The dotted-dashed curves are the experimental spectra.

are used in Eq. (13), with two limits (as discussed in the next two paragraphs) to the transmission function, to obtain the emission spectrum. For the corresponding blackbody emission, we repeat the procedure with $\rho(\omega)$ replaced by the free-space DOS and with $\Gamma(\lambda)=1$.

The coupling factor depends on experimentally imposed boundary conditions. To estimate the upper emission limit, we consider the best-case scenario of negligible nonradiative losses, so that every photon absorbed by the photonic lattice structure is eventually remitted into a propagating Bloch-mode. We approximate this situation with a maximum coupling factor of $\Gamma_{\max}(\lambda)=1-R(\lambda)$. The solid curves in Fig. 2 show the calculated photonic-crystal emission spectra for this optimal situation at different temperatures. Also plotted are the corresponding blackbody spectra (dashed curves). The figure clearly shows the suppression of photonic lattice emission intensity at the photonic band gaps. More importantly, they indicate a significant increase in intensity at the band edges.

Figure 2 also depicts (with a different vertical scale) the experimentally measured spectra (dotted-dashed curves) for a 6 layer tungsten Lincoln-log structure suspended in vacuum by wires. Nonradiative losses are minimized by having an essentially free-standing structure. The experimental structure was electrically excited by Joule heating. To determine the temperature, the experiment was repeated with blackbody paint coating the central region of the crystal, which then acted as the heating element. Since the blackbody paint behaved essentially as a perfect electrical insulator, it did not change the electrical conductivity of the sample. The temperature was deduced by matching the change in electrical resistivity of the photonic crystal in the two experiments, and using Wein's law for the relationship between temperature and blackbody emission peak. The solid and dotted-dashed curves show relatively good agreement between calculation and experiment in terms of the wavelength and relative magnitude of the intensity peaks. Inhomogeneous broadening is included in the calculation to account for crystal imperfections. A 5 meV broadening is chosen to match the linewidths of the experimental spectra. Comparison of absolute intensity is not possible because of experimental calibration difficulties. The experimental emission peak at ~ 2 μm is absent in the calculated results because the band-structure calculation was terminated at the edge of the second band at ~ 3 μm.

To obtain a lower bound for the photonic-crystal emission, we consider the worst-case scenario where all the photons absorbed by the photonic lattice structure is lost nonradiatively. To approximate this situation, we use a minimum coupling function of $\Gamma_{\min}(\lambda)=1-R(\lambda)-A(\lambda)$, where $A(\lambda)$ is calculated using the complex dielectric constant for tungsten.[17] The solid curves in Fig. 3 for the calculated emission spectra at different temperatures, show that for the most part, photonic-crystal emission is at or slightly below the blackbody emission (dashed curves). Comparison with the solid curves in Fig. 2 reveals noticeable spectral shape differences, that are also observed in experiments (compared dotted-dashed curves in Figs. 2 and 3). For the lossy case, the measurements were made with a photonic crystal that is similar to the one used in Fig. 2, but mounted on a heat sink which serves as a channel for nonradiative losses. An inho-

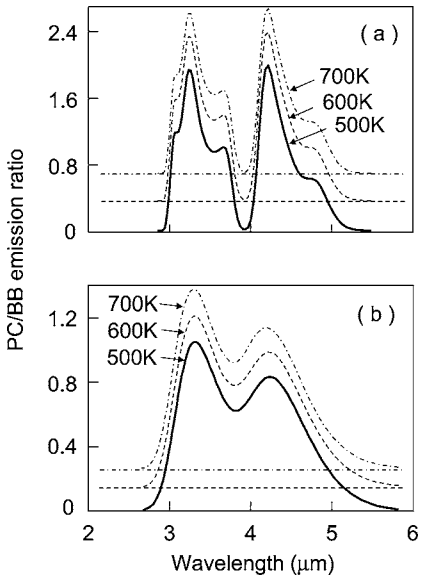

FIG. 4. Ratio of photonic crystal emission to blackbody emission for (a) lossless and (b) lossy cases at different temperatures.

mogeneous broadening of 20 meV is used in the calculation to match the experimental linewidths. The general agreement between theory and experiment provides some assurance of the accuracy of the transmission coupling functions used in the study.

Figures 4(a) and 4(b) are plots of the ratio between photonic-lattice and blackbody emission for the lossless and lossy cases. In both cases, the curves (displaced vertically for clarity) show the independence of the ratio on temperature, indicating that modifications to the emission by the photon lattice under low excitation and rapid equilibration conditions arise mainly from changes in the photon density of states. Therefore, it is unnecessary to excite an active photon-crystal structure to an extreme temperature to see the predicted effects.

Lastly, we note that inhomogeneous broadening plays an important role in determining the shape and amplitude of the photonic-crystal spectrum. This is the case because of the sharpness of the emission peaks in both lossless and lossy structures. Figure 5 illustrates the dependence of the lossy photonic-crystal spectrum on inhomogeneous broadening. Figures 5(a) and 5(b) show that greater than one photonic-crystal to blackbody intensity ratio is possible even in the lossy structure for inhomogeneously broadening of up to 10 meV. However, when both absorption losses and structural aperiodicities are present the photonic-crystal emission peaks are likely to no longer exceed the blackbody emission, as shown in Fig. 5(c).

IV. CONCLUSION

In summary, the emission from an active photonic-lattice crystal is investigated using a model consisting of an inhomogeneously broadened ensemble of two-level systems interacting with a quantized radiation field whose modal properties are determined by the photonic-lattice band structure.

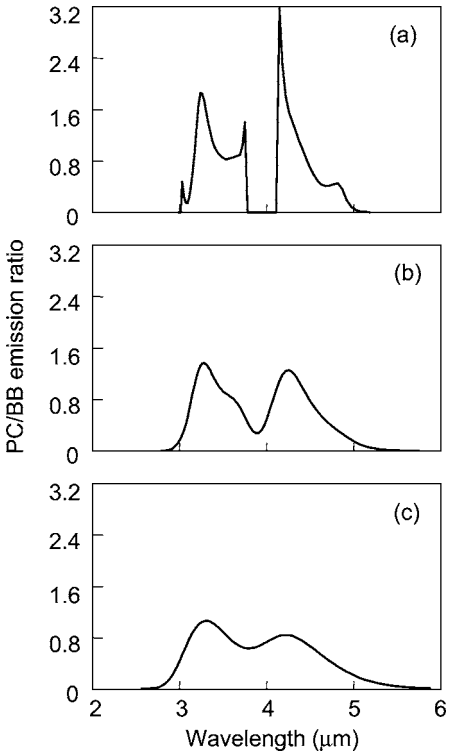

FIG. 5. Ratio of photonic crystal emission to blackbody emission for the lossy case and inhomogeneously broadening of (a) 0, (b) 10, and (c) 20 meV.

The model gives the emission spectra for arbitrary photonic-lattice configurations, and reproduces Planck's radiation formula for thermal emission into free space. Comparison of photonic-lattice and blackbody emission shows appreciable modification of the blackbody spectrum by the photonic lattice, where the redistribution of the photonic density of states results in suppression of emission at certain wavelengths and enhancement at others. Under low excitation and rapid relaxation conditions, the enhancement can give rise to exceedingly high emission peaks at the photonic lattice band edges, with peak intensities exceeding those of a blackbody at the same temperature and wavelength. However, imperfections, such as those resulting in inhomogeneous broadening, absorption and diffraction losses, can negate the excess emission. Our comparison is between an isolated active photonic crystal system and an isolated blackbody system. The results do not apply to situations involving the coupling of the two systems.[9] There, the interaction between the photonic crystal and blackbody (e.g., leading to population distribution changes) should be taken into account. Finally, the parameter space explored excludes situations involving nonequilibrium population effects, even though these effects can be treated within the framework of the present model.

ACKNOWLEDGMENTS

This work was supported by the U. S. Department of Energy under Contract No. DE-AC04-94AL85000 and the Forschungspreis from the Alexander von Humboldt Foundation.

[1] E. Yablonovitch, Phys. Rev. Lett. **58**, 2059 (1987).
[2] S. John and J. Wang, Phys. Rev. Lett. **64**, 2418 (1990).
[3] S. John and J. Wang, Phys. Rev. B **43**, 12772 (1991).
[4] G. Subramania, S. Y. Lin, J. R. Wendt, and J. M. Rivera, Appl. Phys. Lett. **83**, 4491 (2003).
[5] O. Painter, R. K. Lee, A. Scherer, A. Yariv, J. D. O'Brien, P. D. Dapkus, and I. Kim, Science **284**, 1819 (1999).
[6] C. M. Cornelius and J. P. Dowling, Phys. Rev. A **59**, 4736 (1999).
[7] S. Y. Lin, J. G. Fleming, E. Chow, J. Bur, K. K. Choi, and A. Goldberg, Phys. Rev. B **62**, R2243 (2000).
[8] J. G. Fleming, S. Y. Lin, and I. El-Kady, Appl. Phys. Lett. **83**, 593 (2003).
[9] T. Trupke, P. Würfel, and M. A. Green, Appl. Phys. Lett. **84**, 1997 (2004).
[10] N. Vats, S. John, and K. Busch, Phys. Rev. A **65**, 043808 (2002).
[11] M. O. Scully and M. S. Zubairy, *Quantum Optics* (Cambridge University Press, Cambridge, 1977).
[12] For a textbook discussion see A. E. Siegman, *Lasers* (University Science Books, Mill Valley, 1986), Chap. 24.
[13] W. E. Lamb, Jr., Phys. Rev. **134**, A1429 (1964).
[14] M. Sargent, III, M. O. Scully, and W. E. Lamb, Jr., *Laser Physics* (Addison-Wesley, Reading, 1974).
[15] L-L. Lin, Z.-Y. Li, and K.-M. Ho, J. Appl. Phys. **94**, 811 (2003).
[16] Z.-Y. Li and K.-M. Ho, Phys. Rev. B **67**, 165104 (2003).
[17] D. R. Lide, *Handbook of Chemistry and Physics*, 83rd ed. (CRC Press, Boca Raton, 2003).